



Article

Multiwalled Carbon Nanotubes-CeO₂ Nanorods: A “Nanonetwork” Modified Electrode for Detecting Trace Rifampicin

Na Zhang¹, Mariela Brites Helu², Keying Zhang^{1,*}, Xia Fang¹, Hu Yin¹, Jinmin Chen¹, Shangshang Ma¹, Aidong Fang¹ and Cong Wang¹

¹ Anhui Key Laboratory of Spin Electron and Nanomaterials, School of Chemistry and Chemical Engineering, Suzhou University, Suzhou 234000, China; szxyzn@163.com (N.Z.); z2006590@163.com (X.F.); yh17605546701@163.com (H.Y.); jmchen@ahszu.edu.cn (J.C.); shangshangma@ahszu.edu.cn (S.M.); fad5006@163.com (A.F.); szxywangcong@163.com (C.W.)

² Laboratoire de Chimie Physique et Microbiologie pour l'Environnement (LCPME), UMR 7564, CNRS—Université de Lorraine, 54600 Villers-les-Nancy, France; mariela.brites-helu@univ-lorraine.fr

* Correspondence: szxyzky2009@ahszu.edu.cn

Received: 3 January 2020; Accepted: 18 February 2020; Published: 23 February 2020



Abstract: Herein, a “nanonetwork” modified electrode was fabricated based on multiwalled carbon nanotubes and CeO₂ nanorods. Scanning electron microscopy, X-ray powder diffraction and zeta potential were employed to characterize this electrode. Multiwalled carbon nanotubes negatively charged and CeO₂ nanorods positively charged form “nanonetwork” via electrostatic interaction. The performance of the CeO₂ nanorods-based electrode remarkably improved due to the introduction of multiwalled carbon nanotubes. The detection of rifampicin (RIF) was used as a model system to probe this novel electrode. The results showed a significant electrocatalytic activity for the redox reaction of RIF. Differential pulse voltammetry was used to detect rifampicin, the reduction peak current of rifampicin linear with the logarithm of their concentrations in the range of 1.0×10^{-13} – 1.0×10^{-6} mol/L, The linear equation is $i_p = 6.72 + 0.46 \lg c$, the detect limit is 3.4×10^{-14} mol/L ($S/N = 3$). Additionally, the modified electrode exhibits enduring stability, excellent reproducibility, and high selectivity. This strategy can be successfully used to detect trace rifampicin in samples with satisfactory results.

Keywords: multiwalled carbon nanotubes; CeO₂ nanorods; nanonetwork; rifampicin; modified electrode

1. Introduction

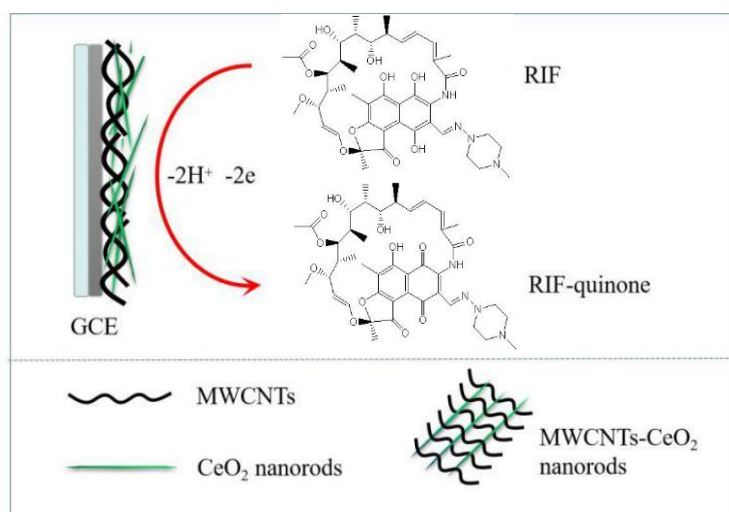
Rifampicin (RIF) (3-[[[4-methyl-1-piperazinyl]imino]methyl]rifamycin), a bactericidal agent, is an important antibiotic drug that is often used to prevent the development of clinical tuberculosis [1]. Moreover, it has important applications in biological and pharmaceutical fields. Recent research demonstrates its efficiency in treating serious infections, such as human immunodeficiency virus (HIV) and cancer [2]. In the body, RIF is mainly metabolized in the liver through deacetylation and excreted in bile together with its metabolites [3]. RIF must be used with caution in the treatment of patients with liver diseases. Therefore, the development of more sensitive methods to detect RIF in pharmaceutical products and biological fluids is highly desired.

Several methods have been reported for detecting RIF, such as high performance liquid chromatography [4], real-time polymerase chain reaction [5], chemiluminescence [6] and fluorescence spectroscopy [7–9]. Although these methods are generally quite sensitive and accurate, they are often costly, technically complex, time-consuming, and do not allow high throughput analysis. Recently, electrochemical methods, especially electrochemical RIF (rifampicin) sensors [10–17], have gained

attention due to their outstanding merits, which includes the simplicity of the sample preparation, low cost of instrumentation, easy miniaturization, high sensitivity and selectivity. In particular, sensors based on metal oxide nanomaterials are well known for their excellent electrical, optical, thermal and catalytic properties, and large surface-to-volume ratio [18,19]. Cerium oxide (CeO_2), an important rare earth material, is commonly seen in sensing due to its good biocompatibility, high stability and remarkable absorption capability [20]. In recent years, various morphologies of CeO_2 including nanoparticles, nanorods, nanocubes, nanoshuttles, and nanoplates, have been synthesized seeking the enhancement of particular properties. For example, Kang et al. reported that CeO_2 nanorods have a forceful adsorption capacity [21]. However, the low conductivity of CeO_2 limits its further application in electrochemical sensing. Thus, it is highly desired to improve the conductivity of CeO_2 -based electrode for constructing electrochemical sensors.

In that sense, multiwalled carbon nanotubes (MWCNTs) are proposed for modifying and improving the performance of CeO_2 -based sensors. MWCNTs offer a large surface area, high mechanical strength, small diameter, good chemical and thermodynamic stability, and most importantly, excellent conductivity. MWCNTs can promote electron transport and increase the electrode surface area in electrochemical sensors as has been reported [22,23].

In this study, we combine the excellent properties of MWCNTs with the absorption capability of CeO_2 nanorods to prepare an electrochemical RIF sensor with enhanced performance (Scheme 1). CeO_2 nanorods with positive electrical charge are mixed with negatively charged MWCNTs to obtain a “nanonetwork” modified film. The results indicate that the “nanonetwork” increases the electrocatalytic activity for the oxidation and reduction of RIF. Moreover, the sensitivity is also increased, allowing to measure traces of RIF with satisfactory accuracy.



Scheme 1. The scheme of the “nanonetwork” modified electrode and its electrocatalytic ability for the oxidation and reduction of RIF.

2. Materials and Methods

2.1. Reagents and Characterization

MWCNTs (purity >95%, diameter 20–30 nm, length 30 mm) were obtained from (Zhongke Nano New Material Co., Ltd., Shenzhen, China), $\text{CeCl}_3 \cdot 7\text{H}_2\text{O}$ was purchased from Sigma (Shanghai, China), RIF (USP grade), 0.1 M phosphate buffer solutions (PBS). Solution with different pH values were prepared by mixing the stock standard solution of Na_2HPO_4 and NaH_2PO_4 and pH was adjusted with H_3PO_4 or NaOH solution. All chemicals were analytical grade and were employed without further purification. Double distilled water was used in the all experiments.

The scanning electron microscope (SEM) images were obtained by Hitachi S-3000N (Japan Hitachi Co., Ltd., Tokyo, Japan); X-ray powder diffraction (XRD) measurements were performed on a Japan Shimadzu XRD-6000 diffractometer (Jiangsu, China) with Cu-K α radiation ($\lambda = 0.15418$ nm) and a scanning rate of 0.05 deg. s^{-1} ; Zeta potentials were measured on a Nano-Z Zetasizer (Malvern Panalytical, Shanghai, China); Electrochemical measurements were carried out using CHI660A electrochemical workstation (Shanghai Chenhua Instrument Co., Ltd., Shanghai, China) with a three-electrode system (Nano-network" Modified Electrode as working electrode, platinum wire as the counter electrode and saturated calomel electrode (SCE) as reference electrode). All electrochemical measurements were carried out in a 10 mL electrochemical cell, where O₂ was removed by bubbling high-purity N₂ for 20 min. A continuous flow of N₂ was maintained over the solution to avoid re-dissolution of O₂ during measurements. All potentials given in this paper are referred to SCE. Each measurement was repeated three times to report statistical values.

2.2. Preparation of CeO₂ Nano-Rods

CeO₂ nanorods were synthesized as reported in previous work [24]. Briefly, 2.0 g CeCl₃·7H₂O was dissolved in 10 mL water (solution a), 3.2 g NaOH was dissolved in 25 mL water (solution b), then both were mixed and stirred for 10 min. The solution was transferred to the reaction vessel and kept at 140 °C for 20 h. The product was rinsed with water and dried at room temperature for 20 h and calcined at 300 °C for 4 h to obtain CeO₂ nanorods.

2.3. Preparation of MWCNTs-CeO₂ Nano-Rods/GCE

A bare, glassy carbon electrode (GCE) was polished to a smooth, mirror-like finish with Al₂O₃ suspension, and cleaned by sonication in anhydrous EtOH and water for 1 min, each. Finally, the electrode was rinsed three times with water and dried at RT. The MWCNTs were used as received, MWCNTs/CeO₂ nanorods suspensions were prepared with different ratios (1:4, 1:2, 1:1, 2:1, 3:1, weight ratios) by sonication during 30 min). The MWCNTs-CeO₂ nanorods/GCE was prepared by drop-casting. Ten μ L of suspension was dropped onto the GCE surface and dried at RT.

3. Results and Discussion

3.1. SEM Characterization of MWCNTs-CeO₂ Nano-Rods Composites

Figure 1 shows the SEM images of CeO₂ nanorods and MWCNTs-CeO₂ nanorods "network" film. It can be seen from Figure 1A, MWCNTs were long and prone to entanglement. Figure 1B showed that the size of CeO₂ nanorods were uniform, the zeta potential measurements showed that CeO₂ nanorods were of the positive charge ($\approx +28$ mV). The XRD was used to characterize the CeO₂ nanorods; these peaks matched the standard JCPDS No. 34-0394 (Figure 1D), indicating that CeO₂ nanorods were successfully fabricated. Figure 1C showed the SEM image of MWCNTs-CeO₂ nanorods film. Compared with the SEM of (A) and (B), the MWCNTs-CeO₂ nanorods were dispersed and capable of forming a uniform "network" film.

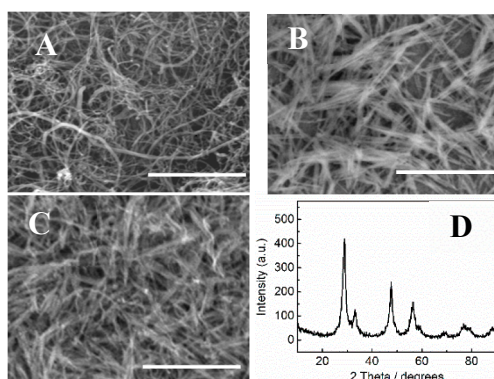


Figure 1. Scanning electron microscope (SEM) images of MWCNTs (A), CeO₂ nanorods (B), and MWCNTs-CeO₂ nanorods (C). Scale bar: 1.0 μm. The XRD of CeO₂ nanorods (D).

3.2. Electrochemical Behaviors of RIF on Different Electrodes

Figure 2 shows several scans of cyclic voltammetry (CV) recorded on 10⁻⁶ mol/L RIF in 0.1 M PBS (pH = 7.0) at different electrodes material: bare GCE (a), CeO₂ nanorods/GCE (b), MWCNTs/GCE (c), and MWCNTs-CeO₂ nanorods/GCE (d). Bare GCE shows virtually no redox activity for RIF as the CV scan does not show a peak pair in curve 2-a. By modifying the electrode with MWCNTs and CeO₂ nanorods, the peaks for the reversible oxidation and reduction of RIF appears, which is evidence of the enhancement on the activity. For CeO₂ nanorods/GCE and MWCNTs/GCE, the oxidation peak appears ca. -0.1 V vs. SCE followed by a reduction peak ca. 0.05 V vs. SCE in the reverse scan. The peak currents are further increased on MWCNTs-CeO₂ nanorods /GCE (curve 2-d). In this case, it is also seen a shift in the peak potential to more negative values. This may be due to: (1) MWCNTs and CeO₂ nanorods have large area which can increase the effective surface area of the electrode, which yield to more activation sites for the reaction of RIF, (2) MWCNTs with good electrical conductivity can improve the electron transfer ability of the electrode; (3) CeO₂ nanorods can increase the adsorption amount of RIF on the modified electrode surface due to its ability to bind to oxygen-rich groups, which could improve the detection signal as well.

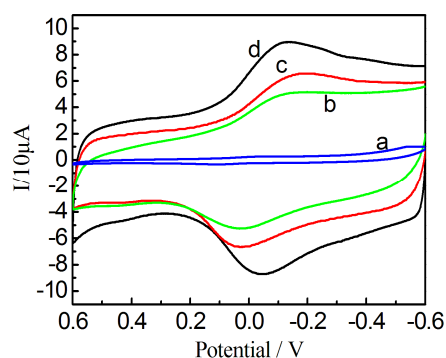


Figure 2. CVs of RIF on the different electrodes: Bare GCE (a); CeO₂ nanorods/GCE (b); MWCNTs/GCE (c); MWCNTs-CeO₂ nanorods/GCE (d) in 0.1 M phosphate buffffer solutions (PBS) (pH = 7.0). Scan rate: 0.10 V/s; the concentration of RIF: 1 × 10⁻⁶ mol/L.

3.3. Optimization of the Ratio of MWCNTs/CeO₂ Nano-Rods

The ratio of MWCNTs/CeO₂ nanorods is a key factor that affects the electrocatalytic activity of the modified electrode. Figure 3 shows the effect of the ratio on the current peak magnitude. The composite with a weight ratio 2:1 exhibits the major enhancement on the activity. Therefore, this composition was selected to further investigate the performance of MWCNTs-CeO₂ nanorods/GCE.

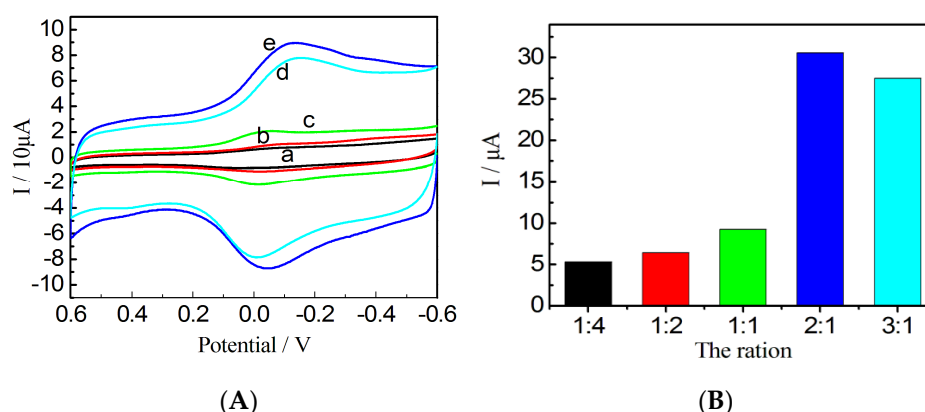


Figure 3. (A) CVs of the electrode modified with different ratio of MWCNTs/CeO₂ nanorods: 1:4 (a); 1:2 (b); 1:1 (c); 2:1 (e); 3:1 (d). (B) The relationship between the reduction peak current and the ratio of MWCNTs/CeO₂ nanorods.

3.4. Effect of pH

The effect of the pH of the solution on the electrochemical response of RIF was investigated by CV. Figure 4 shows scans of MWCNTs-CeO₂ nanorods/GCE-RIF carried out under different pH conditions within the range of 5.0–9.0. Both, the current and the potential peaks are affected by the pH. As shown in Figure 4B the reduction peak current of RIF reaches its maximum value in neutral solutions (pH = 7). Thus, PBS buffer has to be added to maintain the pH at 7 during the measurements. In addition, the anodic and cathodic peaks shift to more negative values when the pH increases. This has a clear linear relationship, as shown in Figure 4C. The linear regression equation is $E_{pa} = 0.51 - 0.072\text{pH}$ ($R^2 = 0.9862$) for the anodic process and $E_{pc} = 0.34 - 0.066\text{pH}$ ($R^2 = 0.9859$) for the cathodic process. These results show the participation of protons in the electrochemical reaction mechanism. The path for the reaction is shown in Scheme 1. Similar results and hypothesis were reported in previous work [10] (Scheme 2).

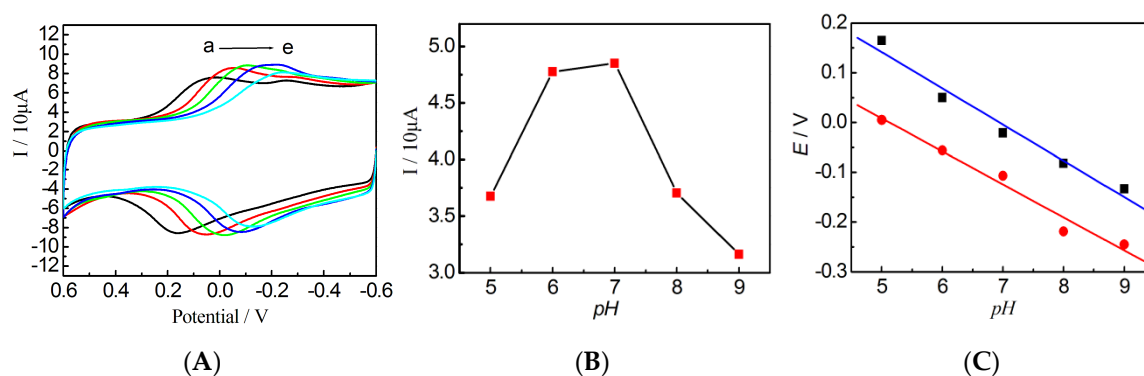


Figure 4. (A) CVs of RIF at the MWCNTs-CeO₂ nanorods/GCE in 0.1 M PBS with different pH (a—5.0, b—6.0, c—7.0, d—8.0, e—9.0); (B) The relationship between the reduction peak current and pH; (C) The relationship between the peak potential and pH (The reduction peak potential (blue) and The oxidation peak potential (red)). Scan rate: 0.10 V/s.

decreased thousands of times, positioning the MWCNTs-CeO₂ nanorods/GCE sensor as a promising tool in assay RIF in biological and pharmaceutical samples.

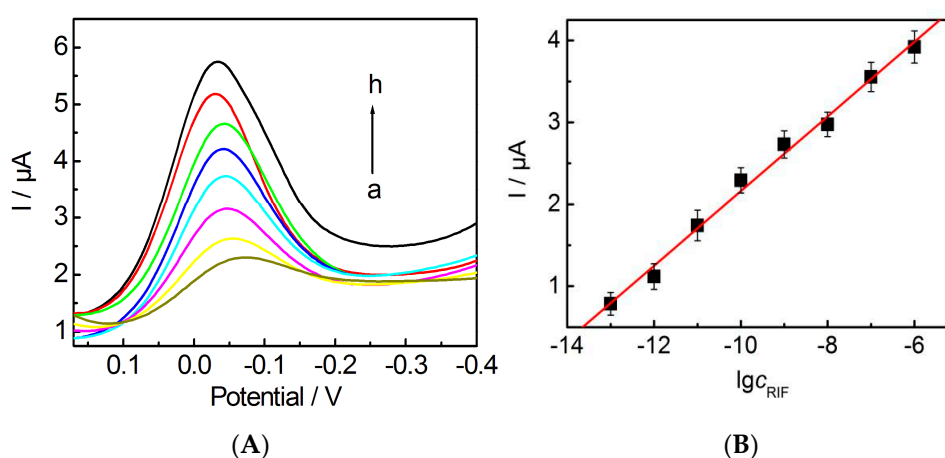


Figure 6. (A) DPVs of the different concentrations of RIF at MWCNTs-CeO₂ nanorods/GCE in 0.1 mol/L PBS (pH = 7.0); (B) The reduction peak current vs. the concentration of RIF. a— 1.0×10^{-13} , b— 1.0×10^{-12} , c— 1.0×10^{-11} , d— 1.0×10^{-10} , e— 1.0×10^{-9} , f— 1.0×10^{-8} , g— 1.0×10^{-7} , h— 1.0×10^{-6} mol/L.

Table 1. Comparison of the linear ranges and detection limits of previous RIF sensors.

Modified Electrode	Linear Range (mol/L)	Detection Limit (mol/L)	Ref.
Gold nanoparticles/poly-melamine nanocomposite	8.0×10^{-8} – 1.5×10^{-5}	3.0×10^{-8}	[12]
Graphene nanoplatelets	1.0×10^{-9} – 1.0×10^{-4}	5.0×10^{-10}	[13]
Copper metal organic framework/mesoporous carbon	8.0×10^{-8} – 8.5×10^{-5}	2.8×10^{-10}	[15]
MWCNTs/meso-tetrakis(4-hydroxyphenyl) porphyrinato cobalt(II)	1.0×10^{-8} – 5.0×10^{-3}	8.0×10^{-9}	[17]
MWCNTs-CeO ₂ nanorods/GCE	1.0×10^{-13} – 1.0×10^{-6}	3.4×10^{-14}	This work

3.7. Reproducibility and Stability of Modified Electrode

The reproducibility and stability of modified electrode was studied. Three MWCNTs-CeO₂ nanorods/GCE were independently prepared and employed to detect the same reference solution of RIF with a concentration of 1.0×10^{-9} mol/L. The relative standard deviation found was equal to 3.7%, which indicates that the modified electrode has an excellent reproducibility. In addition, the modified electrode was kept in 0.1 mol/L PBS for 4 consecutive days at room temperature and used for measuring the reference solution, once a day. The electrochemical signal was quite stable during this period with values that represent the 97%, 93%, 91%, and 90% of the original measured value.

3.8. Interference Studies and Samples Analysis

Several concomitants were added to the RIF solution to study their interference during the detection of RIF. Uric acid, *L*-threonine, and glucose were selected as potential interference to evaluate the selectivity of the modified electrode for detecting RIF in pharmaceutical formulations and the biological fluids. The test results indicate that concentration of uric acid, *L*-threonine and glucose up to 600-fold the RIF concentration do not have an effect on the DPV detection signal of RIF. Therefore, the MWCNTs-CeO₂ nanorods/GCE sensor can be used to determine RIF in human serum. Analysis of complex samples by the standard addition method were carried out. The recovery data is shown in Table 2. The values are in the range of 94.6–102.2%, indicating the constructed method can be applied to detect RIF in the complex samples.

Table 2. Determination of RIF in serum samples ($n = 3$).

Sample	Added (pmol L ⁻¹)	Found (pmol L ⁻¹)	Recovery (%)	R.S.D. (%)
1	1.0	0.97	97.0	1.97
2	10.0	9.46	94.6	1.87
3	50.0	51.1	102.2	2.02

4. Conclusions

Herein, a “nanonetwork” modified electrode was fabricated based on MWCNTs and CeO₂ nanorods, and employed to detect RIF. The electrochemical behavior and reaction mechanism of RIF at this modified electrode surface was studied. The experiment results imply that the proposed electrode have obvious electrocatalytic ability for the redox of RIF. Additionally, the proposed method has high sensitivity and selectivity, and has been successfully applied for detecting RIF in complex samples, thus demonstrating its potential application in the assay of RIF in biological and pharmaceutical samples.

Author Contributions: N.Z., X.F., and H.Y.: conceptualization, investigation; J.C., S.M.: original draft preparation; A.F. and C.W.: editing of figures; K.Z.: conceptualization, supervision, writing—review and editing; M.B.H.: writing, review and editing. All authors have read and agreed to the published version of the manuscript.

Funding: We gratefully appreciate financial support from the Key Project of Anhui Province Excellent Talent Support Program (gxyqZD2019079); PhD Research Funding of Suzhou University (2019jb27); the funded project of Anhui Province Cultivate Outstanding Talent (No. 2014SQR01); the Natural Science Research Key Project of Education Department of Anhui Province (KJ2017A434, KJ2019A1001, KJ2019A0671); the Open Research Project of Suzhou University Research Platform (2019ykf08, 2019ykf08); and the National University Student Innovation and Entrepreneurship Project (201910379022).

Conflicts of Interest: The authors declare no conflict of interest.

References

- Panchagnula, R.; Agrawal, S. Rapid dissolving high potency danazol powders produced by spray freezing into liquid process. *Int. J. Pharm.* **2004**, *271*, 145–154.
- Ali, M.R.K.; Panikkanvalappil, S.R.; El-Sayed, M.A. Enhancing the efficiency of gold nanoparticles treatment of cancer by increasin their rate of endocytosis and cell accumulation using rifampicin. *J. Am. Chem. Soc.* **2014**, *136*, 4464–4467. [[CrossRef](#)]
- Allen, J.L.; Marriner, G.A.; Via, L.E.; Barry, C.E.; Caprioli, R.M. Absolute quantitative maldi imaging mass spectrometry: A case of rifampicin in liver. *Anal. Chem.* **2016**, *88*, 2392–2398.
- Umang, S.; Shraddha, P.; Manan, R. Stability indicating reverse phase HPLC method for estimation of rifampicin and piperine in pharmaceutical dosage form. *Curr. Drug Discov. Technol.* **2018**, *11*, 54–64.
- Sahebi, L.; Khalil, A.; Monfaredan, A.; Farajnia, S.; Nili, S.; Khalili, M. Rapid detection of rifampicin- and isoniazid-resistant mycobacterium tuberculosis using real-time PCR. *Jundishapur J. Microbiol.* **2016**, *9*, e29147. [[CrossRef](#)]
- Ma, Y.; Zhang, B.T.; Zhao, L.X.; Guo, G.S.; Lin, J.M. Determination of rifampicin by peroxomonosulfate-cobalt(II) chemiluminescence system. *Chin. J. Chem.* **2008**, *26*, 905–910. [[CrossRef](#)]
- Wu, X.M.; Zhang, J.H.; Feng, Z.S.; Chen, W.X.; Zhang, F.; Li, Y. An ultra-sensitive “turn-off” fluorescent sensor for the trace detection of rifampicin based on glutathione-stabilized copper nanoclusters. *Analyst* **2020**. [[CrossRef](#)] [[PubMed](#)]
- Su, J.; Xiang, X.F.; Lv, R.; Li, H.; Fu, X.; Yang, B.Y.; Gu, W.; Liu, X. Rapid and high-selectivity detection of rifampicin based on upconversion luminescence core-shell structure composites. *J. Solid State Chem.* **2018**, *266*, 9–15. [[CrossRef](#)]
- Liu, Z.Q.; Yin, P.F.; Gong, H.P.; Li, P.P.; Wang, X.D.; He, Y.Q. Determination of rifampicin based on fluorescence quenching of GSH capped CdTe/ZnS QDs. *J. Lumin.* **2012**, *132*, 2484–2488. [[CrossRef](#)]
- Asadpour-Zeynali, K.; Mollarasouli, F. Novel electrochemical biosensor based on PVP capped CoFe₂O₄@CdSe core-shell nanoparticles modified electrode for ultra-trace level determination of rifampicin by square wave adsorptive stripping voltammetry. *Biosens. Bioelectron.* **2017**, *92*, 509–516. [[CrossRef](#)] [[PubMed](#)]

11. Shiri, S.; Pajouheshpoor, N.; Khoshshafar, H.; Amidi, S.; Bagheri, H. An electrochemical sensor for the simultaneous determination of rifampicin and isoniazid using a C-dots@CuFe₂O₄ nanocomposite modified carbon paste electrode. *New J. Chem.* **2017**, *41*, 15564–15573. [[CrossRef](#)]
12. Amidi, S.; Hosseinzadeh Ardakani, Y.; Amiri-Aref, M.; Ranjbarib, E.; Sepehri, Z.; Bagheri, H. Sensitive electrochemical determination of rifampicin using gold nanoparticles/poly-melamine nanocomposite. *RSC Adv.* **2017**, *7*, 40111–40118. [[CrossRef](#)]
13. Zou, J.; Huang, L.L.; Jiang, X.Y.; Jiao, F.P.; Yu, J.G. Electrochemical behaviors and determination of rifampicin on graphene nanoplatelets modified glassy carbon electrode in sulfuric acid solution. *Desalin. Water Treat.* **2018**, *120*, 272–281. [[CrossRef](#)]
14. Huang, Q.; Li, X.K.; Feng, S.X.; Zhuge, W.F.; Liu, F.P.; Peng, J.Y.; Mo, S.C. An electrochemical sensor based on the composite of molybdenum carbides and a multiwalled carbon nanotube modified electrode for the ultrasensitive detection of rifampicin. *Anal. Methods* **2018**, *10*, 3594–3601. [[CrossRef](#)]
15. Oliveira, P.R.; Schibelbain, A.F.; Neiva, E.G.C.; Zarbin, A.J.G.; Marcolino-Junior, L.H.; Bergamini, M.F. Nickel hexacyanoferrate supported at nickel nanoparticles for voltammetric determination of rifampicin. *Sens. Actuators B Chem.* **2018**, *260*, 816–823. [[CrossRef](#)]
16. Rawool, C.R.; Srivastava, A.K. A dual template imprinted polymer modified electrochemical sensor based on Cu metal organic framework/mesoporous carbon for highly sensitive and selective recognition of rifampicin and isoniazid. *Sens. Actuators B Chem.* **2019**, *288*, 493–506. [[CrossRef](#)]
17. Sonkar, P.K.; Yadav, M.; Prakash, K.; Ganesan, V.; Sankar, M.; Yadav, D.K.; Gupta, R. Electrochemical sensing of rifampicin in pharmaceutical samples using meso-tetrakis (4-hydroxyphenyl)porphyrinato cobalt(II) anchored carbon nanotubes. *J. Appl. Electrochem.* **2018**, *48*, 937–946. [[CrossRef](#)]
18. George, M.; Antony, A.; Mathew, B. Metal oxide nanoparticles in electrochemical sensing and biosensing: A review. *Microchim. Acta* **2018**, *185*, 358–364. [[CrossRef](#)]
19. Kempahanumakkagari, S.; Deep, A.; Kim, K.H.; Kailasa, S.K.; Yoon, H.O. Nanomaterial-based electrochemical sensors for arsenic—A review. *Biosens. Bioelectron.* **2017**, *95*, 106–116. [[CrossRef](#)]
20. Malhotra, B.D.; Kaushik, A. Metal oxide-chitosan based nanocomposite for cholesterol biosensor. *Thin Solid Films* **2009**, *518*, 614–620. [[CrossRef](#)]
21. Kang, D.J.; Yu, X.L.; Ge, M.F. Morphology-dependent properties and adsorption performance of CeO₂ for fluoride removal. *Chem. Eng. J.* **2017**, *330*, 36–43. [[CrossRef](#)]
22. Wang, Z.H.; Yu, J.B.; Gui, R.J.; Jin, H.; Xia, Y.Z. Carbon nanomaterials-based electrochemical aptasensors. *Biosens. Bioelectron.* **2016**, *79*, 136–149. [[CrossRef](#)] [[PubMed](#)]
23. Li, X.J.; Ping, J.F.; Ying, Y.B. Recent developments in carbon nanomaterial-enabled electrochemical sensors for nitrite detection. *TRAC Trends Anal. Chem.* **2019**, *113*, 1–12. [[CrossRef](#)]
24. Qian, X.C.; Qu, Q.; Li, L.; Ran, X.; Zu, L.M.; Huang, R.; Wang, Q. Ultrasensitive electrochemical detection of clostridium perfringens DNA based morphology-dependent DNA adsorption properties of CeO₂ nanorods in dairy products. *Sensors* **2018**, *18*, 1878. [[CrossRef](#)] [[PubMed](#)]

